Acta Cryst. (1998). B**54**, 365–375

Structural Investigation of $P_4W_{24}O_{80}$: A New Monophosphate Tungsten Bronze

Pascal Roussel,[a]* Glenn Mather,[b] Bernadette Domengès,[a] Daniel Groult[a] and Philippe Labbé[a]

[a]*Laboratoire CRISMAT, CNRS UMR 6508, ISMRA Bd du Maréchal Juin, 14050 Caen CEDEX, France, and* [b]*Departamento de Engenharia Ceramica e do Vidro, Universidade de Aveiro, 3800 Aveiro, Portugal.*
E-mail: p.roussel@crismat.ismra.fr

(*Received 28 September 1997; accepted 1 December 1997*)

Abstract

The crystallographic study of the tungsten phosphate bronze $P_4W_{24}O_{80}$ was performed from three-dimensional single-crystal X-ray diffraction data and electron microscopy. This compound crystallizes in the orthorhombic system with unit-cell dimensions a = 5.312 (1), b = 6.5557 (8), c = 42.196 (8) Å and space group $P2_12_12_1$. The crystal structure was solved by direct methods and Fourier techniques, and refined to the reliability factor R = 0.0284 (wR = 0.0272). Its determination confirms that it belongs to the monophosphate tungsten bronze family of the general formula $(PO_2)_4(WO_3)_{2m}$ with the value m = 12. Large empty cages surrounded by 18 O atoms are built up of eight WO_6 octahedra and four PO_4 tetrahedra sharing corners. They are located between two WO_3-type slabs forming pentagonal-shaped tunnels running in the **a** direction. Electron microscopy investigations confirm that the studied crystal does not imply modulation phenomena when other crystals of the same composition exhibit satellite reflections with a modulation vector **q*** involving a doubling of **a**. The observations also reveal the existence of a monoclinic form of the m = 12 compound, which is a regular intergrowth of m = 11 and m = 13 members in a similar way to the m = 5 member of the series where the same feature has already been observed. On each edge of a WO_3-type slab, a large variation (from 1.73 to 2.09 Å) of the six W—O distances within the WO_6 octahedron is noted, which yields an oxidation state of W near 6, whereas for the WO_6 octahedra located in the middle part of the slab the six W—O distances are gathered about their mean value (1.92 Å), which involves a more important electronic delocalization. The thermal motion of the W atoms is described. The absolute structural configuration is tested on the basis of some calculated structure factors, which are more sensitive to the $x, y, z \rightarrow -x, -y, -z$ change of atomic positions.

1. Introduction

The monophosphate tungsten bronze series of the general formula $(PO_2)_4(WO_3)_{2m}$ has been the focus of extensive investigation this last decade, because of unusual electronic instabilities which vary with the value of m (Hess *et al.*, 1996; Schlenker *et al.*, 1996). The early members, with $m < 7$ (m = 4, 6), undergo a Peierls transition at low temperature ($T < 100$ K) towards a charge-density wave state (CDW) characterized by a sinusoidal modulation (Foury & Pouget, 1993). Magnetoresistivity and magnetic torque measurements have provided information on the size of the pockets of electrons and holes left on the Fermi surface by the CDW gap opening (Le Touze *et al.*, 1995). For large values of m ($8 \leq m \leq 14$) a rich variety of commensurate and incommensurate modulations is observed with high transition temperatures ($T > 500$ K) (Ottolenghi & Pouget, 1996).

The mechanism at the origin of such instabilities is not clear. From a theoretical point of view, the difference between the low (m = 4, 6) and high ($8 \leq m \leq 14$) members leads one to question (*a*) how the conducting electrons are distributed inside the WO_3-type slabs; (*b*) how the coupling phenomenon evolves in the series; (*c*) how WO_3-type antiferroelectric instabilities can interact with CDW instabilities for $m \leq 14$. In order to answer these questions accurate single-crystal X-ray data are required for band structure calculations. However, this information is not readily available for high m values ($m > 8$). Up to now, only the crystal structures of low m members have been resolved (Giroult *et al.*, 1981; Labbé *et al.*, 1986; Roussel *et al.*, 1996). Following on from these studies, the hidden nesting Fermi-surface concept has been suggested to understand the transport and X-ray diffuse scattering studies of the first members, m = 4, 6 (Canadell & Whangbo, 1991).

In this paper we report on the structure of the m = 12 member of the series. According to X-ray diffuse scattering measurements performed between 15 and 650 K (Ottolenghi & Pouget, 1996), the title phase undergoes two Peierls transitions at temperatures of 535 and 500 K, with the appearance of satellite reflections corresponding to modulation wavevectors $\mathbf{q}_1^*(0.12, 0, 0)$ and $\mathbf{q}_2^*(0.5, 0, 0.5)$, respectively. Superlattice spots with components close to $(\frac{1}{2}, 0, 0)$ can also be observed on electron diffraction patterns ([001] zone axis) at 150 K; these spots disappear at 540 K (Yan *et al.*, 1995). However, another set of satellite spots was observed

ISSN 0108-7681

Table 1. *Experimental details*

Crystal data	
Chemical formula	$P_4W_{24}O_{80}$
Chemical formula weight	5816.2
Cell setting	Orthorhombic
Space group	$P2_12_12_1$
a (Å)	5.312 (1)
b (Å)	6.5557 (8)
c (Å)	42.196 (8)
V (Å^3)	1469.5 (8)
Z	1
D_x (Mg m^{-3})	6.572 (4)
Radiation type	Mo $K\alpha$
Wavelength (Å)	0.71073
No. of reflections for cell parameters	25
θ range (°)	18–24
μ (mm^{-1})	48.184
Temperature (K)	295
Crystal form	Platelet delimited by (010), (110) and (001)
Crystal size (mm)	0.125 × 0.069 × 0.003
Crystal colour	Dark blue
Data collection	
Diffractometer	CAD-4
Data collection method	ω–θ/2 scans
Scan (°)	1 + 0.35tan θ
Absorption correction	Gaussian
T_{min}	0.2509
T_{max}	0.8680
No. of measured reflections	6858
No. of independent reflections	6858
No. of observed reflections	1202
Criterion for observed reflections	$I > 3\sigma(I)$
θ_{max} (°)	45
Range of h, k, l	$0 \rightarrow h \rightarrow 10$ $0 \rightarrow k \rightarrow 13$ $-82 \rightarrow l \rightarrow 0$
No. of standard reflections	3
Frequency of standard reflections (min)	60
Intensity decay (%)	7
Refinement	
Refinement on	F
R	0.0284
wR	0.0272
S	1.80
No. of reflections used in refinement	1202
No. of parameters used	140
Weighting scheme	$w = 1/\sigma^2(F_o)$
$(\Delta/\sigma)_{max}$	0.0007
$\Delta\rho_{max}$ (e Å^{-3})	2.81
$\Delta\rho_{min}$ (e Å^{-3})	−1.84
Extinction method	Isotropic secondary, type II (Becker & Coppens, 1974)
Extinction coefficient	0.49 (6)

around the strong main spots of the perovskite WO_3-type slabs, with components of approximately (0.23, 0.19, 0). The origin of this second set of satellite spots, which are still observed at 540 K, is unclear at present. It should be noted that results are not always reproducible from one sample to the next, as indicated from d.c. resistivity measurements (Hess, 1997). This suggests that the CDW state is either a metastable state or a state which is very sensitive to defects created in the samples. Previous results are compatible with the present detailed structural investigation of two m = 12 single crystals. Since no satellite reflections have been found in these phases, it is more than likely that they are in the conducting normal state.

2. Experimental

2.1. *Crystal growth*

Plate-like blue crystals of $P_4W_{24}O_{80}$ (m = 12) were prepared by the chemical vapour transport technique using the following procedure. A mixture of $(NH_4)_2HPO_4$ and WO_3 was first heated at 873 K in air for 12 h to decompose the ammonium phosphate. An appropriate amount of metallic tungsten in powder form was then added before the mixture was heated in an evacuated silica ampoule at 1273 K for 2 d. A portion of ~2 g of the resulting polycrystalline sample was subsequently taken for crystal growth.

Since the objective of the experiment was the preparation of single crystals of large enough size for physical measurements, crystal growth was carried out in a quartz tube 20 cm long and 1.8 cm internal diameter, which was sealed under vacuum. The tube was introduced in a horizontal furnace and a temperature gradient of ~10 K cm^{-1} was applied along its length, *i.e.* the hot zone = 1473 K and the cold zone = 1273 K. The samples were held under these conditions for 2 weeks. Plate-like blue crystals grew in the intermediate zone of the tube.

2.2. *Electron microscopy study*

In order to characterize the title phase by electron microscopy, crystals from various preparations were gently crushed in an agate mortar in *n*-butanol and deposited on a perforated carbon-coated copper grid. The first single crystal to be studied by X-ray diffraction was individually crushed so that various fragments of this crystal could be studied separately from other crystals. Electron diffraction (ED) was carried out on a JEM200CX equipped with a tilting rotating goniometer (± 60°) in order to perform reconstruction of the reciprocal space. High-resolution studies were conducted using a TOPCON 2B electron microscope equipped with a ±10° double tilt goniometer and an objective lens with a spherical aberration constant of 0.4 mm. Image simulations were performed using the multislice method with an EMS package.

2.3. *Data collection and processing*

The quality of the samples was checked using a Weissenberg camera. For this, numerous crystals were

glued to the tip of a Lindemann capillary. It was found that only two crystals were of a sufficient quality for further investigation. Measurement of the parameters at the zero level ($a \simeq 5.3$, $b \simeq 6.5$, $c \simeq 42.1$ Å) were consistent with the $m = 12$ member of the series. However, no satellite reflections were observed on films rotated about [100], even after long exposure to the X-rays. Although some spots appeared elongated or as doublets, particularly at high θ and for high h levels, no evidence of a twin was found. Furthermore, no significant deviation from 90° appeared for the three lattice angles. It was, therefore, concluded that the symmetry of the title phase is orthorhombic, with only the following systematic conditions limiting the observed reflections: $h00$: $h = 2n$, $0k0$: $k = 2n$ and $00l$: $l = 2n$, in accordance with the space group $P2_12_12_1$. This space group has also been adopted for all other previously studied m-even members, except $m = 2$, *i.e.* WPO_5 (Wang *et al.*, 1989). In this case the space group is $P2_1cn$ if c is the largest lattice parameter and a and b remain unchanged. The diffracted intensities were collected at room temperature on an Enraf–Nonius CAD-4 diffractometer using Mo $K\alpha$ radiation for both samples. The detailed recording conditions for the second crystal are given in Table 1†.

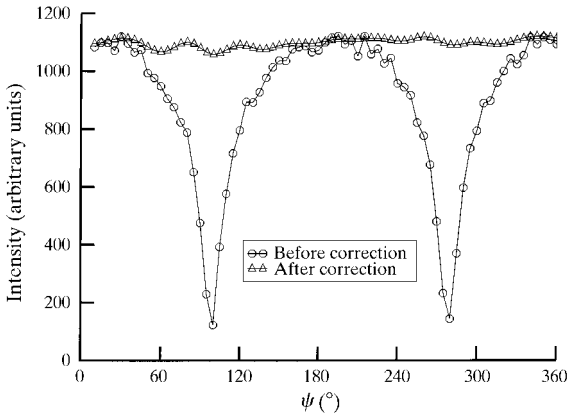

Fig. 1. ψ scan between 0 and 360° for the 600 reflection before and after absorption correction.

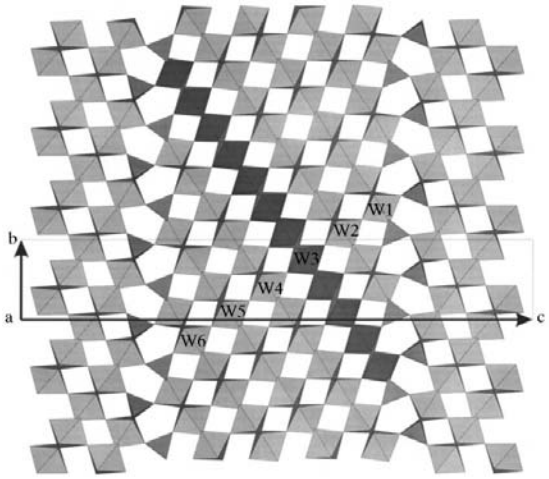

Fig. 2. Projection along **a** of the polyhedral framework showing pentagonal tunnels. The octahedra of the chain noted W(1)–W(6) are approximately at the same level, x, and are all tilted in the same sense. In the perpendicular direction the number of black octahedra corresponds to the $m = 12$ value.

Table 2. *Fractional atomic coordinates and isotropic displacement parameters (Å²)*

	x	y	z	B
W(1)	0.2431 (7)	0.4272 (2)	0.69885 (3)	0.58 (2)†
W(2)	0.251 (1)	0.0996 (2)	0.62523 (3)	0.62 (2)†
W(3)	0.2526 (8)	0.7578 (2)	0.55324 (3)	0.77 (2)†
W(4)	0.2622 (6)	0.4137 (3)	0.48215 (3)	0.67 (2)†
W(5)	0.7626 (7)	0.4299 (2)	0.58941 (3)	0.68 (3)†
W(6)	0.7592 (6)	0.7693 (2)	0.66258 (3)	0.59 (2)†
P	0.762 (3)	0.1144 (8)	0.7243 (1)	0.3
O(1)	0.73 (1)	0.058 (3)	0.7590 (5)	1.3 (3)
O(2)	0.547 (7)	0.263 (5)	0.7170 (8)	1.9 (5)
O(3)	0.025 (5)	0.211 (4)	0.7193 (7)	1.0 (4)
O(4)	−0.022 (5)	0.566 (4)	0.6888 (6)	0.7 (3)
O(5)	0.477 (5)	0.609 (4)	0.6837 (6)	0.6 (3)
O(6)	0.26 (1)	0.258 (3)	0.6649 (5)	1.1 (3)
O(7)	0.537 (6)	0.946 (4)	0.6466 (7)	1.0 (4)
O(8)	1.038 (6)	0.902 (5)	0.6487 (7)	1.4 (5)
O(9)	0.469 (6)	0.269 (4)	0.6064 (6)	1.0 (4)
O(10)	−0.036 (5)	0.244 (3)	0.6166 (5)	0.2 (3)
O(11)	0.269 (8)	−0.066 (3)	0.5920 (4)	0.9 (3)
O(12)	0.547 (6)	0.626 (4)	0.5735 (7)	1.1 (4)
O(13)	1.043 (6)	0.564 (4)	0.5744 (6)	0.9 (4)
O(14)	0.475 (6)	0.935 (4)	0.5321 (5)	1.0 (4)
O(15)	−0.037 (5)	0.898 (4)	0.5412 (5)	0.4 (3)
O(16)	0.233 (6)	0.591 (3)	0.5181 (4)	0.3 (2)
O(17)	0.542 (5)	0.281 (3)	0.4988 (6)	0.1 (3)
O(18)	0.772 (7)	0.256 (4)	0.5556 (6)	1.1 (3)
O(19)	0.778 (7)	0.582 (4)	0.6302 (5)	1.0 (4)
O(20)	0.726 (7)	−0.086 (3)	0.7044 (5)	1.1 (3)

† $B_{eq} = (8\pi^2/3)\Sigma_i\Sigma_j U^{ij} a^i a^j \mathbf{a}_i.\mathbf{a}_j$.

During data reduction of the first crystal, a great number of dubious reflections (1127/25 499 measurements), with a position which deviated from that expected, were rejected. The measured intensities of four symmetrically equivalent reflections were corrected for scale variation based upon standards, and Lorentz and polarization effects. A Gaussian-type absorption correction based on the crystal morphology was then applied. The internal reliability factor $R_{int} = \Sigma_i\Sigma_j(I_j - \bar{I}_j)/\bar{I}_i$, which is related to the *mmm* Laue symmetry, was calculated; values of 0.038, before correction for absorption, and 0.023, after correction, were obtained and, thus, provide further evidence for orthorhombic symmetry.

† A list of structure factors has been deposited with the IUCr (Reference: LC0001). Copies may be obtained through The Managing Editor, International Union of Crystallography, 5 Abbey Square, Chester CH1 2HU, England.

All refinements were carried out using the *JANA*96 program package (Petricek & Dusek, 1997). Scattering factors for neutral atoms and the correction terms for anomalous dispersion were taken from Maslen *et al.* (1992) and Creagh & McAuley (1992), respectively. Atomic parameters, scale factors and isotropic extinction coefficients (Becker & Coppens, 1974) were refined in the full-matrix mode, minimizing the function wR. A weighting scheme based on $\sigma(F_o)$ was used.

The space group $P2_12_12_1$ (no. 19) was found to be compatible with the observed extinction rules. All the W and P atoms were then located with the *SIR*92 direct-methods program (Altomare *et al.*, 1994). The oxygen positions, all except one, were determined from difference-Fourier maps. From previous structural studies of members with lower m values, the host lattice of the $m = 12$ member could be estimated approximately. Visualization of this approximate structure permitted the remaining oxygen to be located. The atomic refinement then rapidly converged to encouraging values (R = 0.05 and wR = 0.04).

However, some of the results were not completely satisfactory. In particular, the thermal B factor of the W atoms remains rather high compared with values found in the crystal structures of other members of the series. This was assumed to be attributable, at least in part, to the high value of the c parameter (c = 42.1 Å) and, consequently, to possible peak-overlap phenomena.

In order to obtain more information on the structure, data collection of the second crystal was considered. Despite its smaller size, and hence a reduced number of data points [1202 hkl with $I > 3\sigma(I)$ rather than 1952], this crystal produced finer spots on Weissenberg films; it was therefore supposed that its reflections may be easier to isolate than those of the larger crystal. Particular attention was paid to adjusting the parameters of the data collection, especially the scan angle, in order to avoid peak-superposition effects. Only one independent space was registered. The size of the crystal plate was determined from an ocular-scaled microscope, taking special care to accurately measure the crystal thickness. The measured shape and dimensions of the crystal were checked by applying an absorption correction to a series of ψ scans taken for 25 reflections. Application of the absorption correction resulted in a decrease of the reliability factor by approximately 0.07, which supports the accurate determination of the morphology of the sample (the effect of correction for absorption on the 600 reflection is given as an example in Fig. 1). The previously observed anomalies disappeared after correction for absorption, but the thermal factor of the P atom always refined to a value close to zero. Final atomic positions are shown in Table 2.

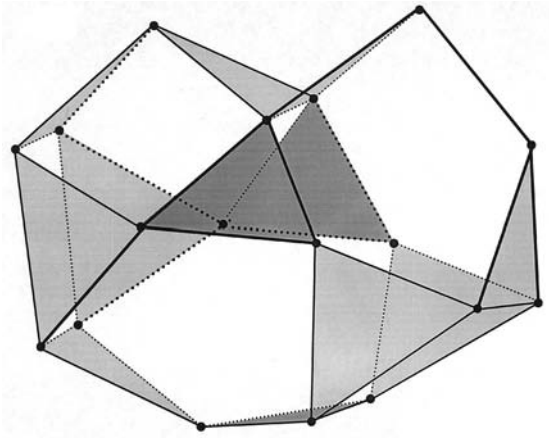

Fig. 3. View of the O_{18} cages along a direction inclined at 10° from **a**. The 18 O atoms are represented by black points. Light shaded areas are WO_6 octahedral faces and dark shaded areas are PO_4 tetrahedral faces. The different O_{18} cages are stacked in the (**a,b**) plane and are bound by the four pentagonal windows.

3. Discussion

3.1. *Description of the crystal structure*

As expected, the crystal structure of $P_4W_{24}O_{80}$ is similar to other members of the $(PO_2)_4(WO_3)_{2m}$ family,

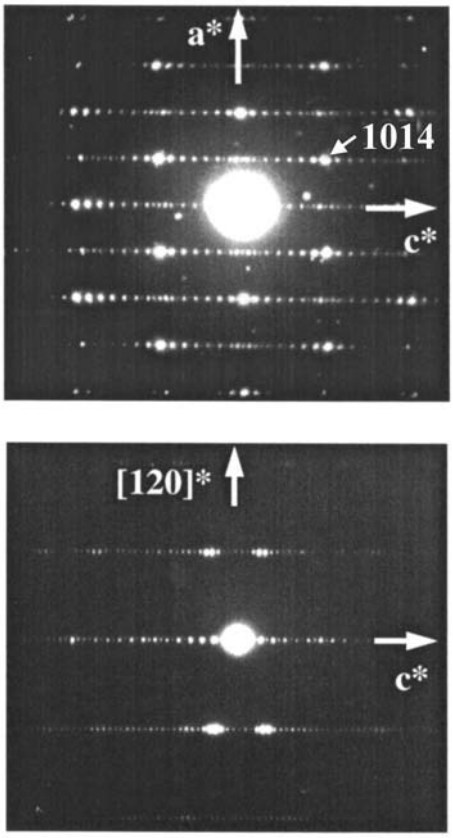

Fig. 4. Two characteristic ED patterns which should show satellites if there were any: *h0l* and *h*2*hl*. For this crystal, no satellite can be seen.

and, in particular, has a polyhedral arrangement closely related to that of the *m*-even members of the series, *i.e.* $m = 2, 4, 6$ and 8. As seen from Fig. 2, the structure is formed by the regular stacking of identical slabs of WO_3-type octahedra along **c**, which are linked to each other by PO_4 tetrahedra arranged in slices parallel to the slabs. Each slab is built up of chains of six corner-sharing WO_6 octahedra [W(1)–W(6) in Fig. 2], which corner-share with four analogous chains of the same length running in the same directions, [092] or [09$\bar{2}$], since two successive slabs are related with a binary screw axis. Within a chain, all the WO_6 octahedra are tilted in the same sense in such a way that the edges of two consecutive WO_6 octahedra make an angle of $\sim$16 (1)° along **a**, while no tilting is observed around the other axes of the octahedra, as previously observed for $P_4W_{14}O_{50}$ (Roussel *et al.*, 1996).

At the end of each chain, the PO_4 tetrahedra share three corners with tetrahedra within the slab and the other corner with the adjacent slab, so that between WO_3 slabs pentagonal-shaped tunnels form which run parallel to the **a** axis (Fig. 2), hence the generic name given to the series, MonoPhosphate Tungsten Bronzes with pentagonal tunnels ($MPTB_p$). However, this description is only partial. Quite large cages of similar size are found between layers which are linked to each other by pentagonal 'windows'; the orthogonal projection in the (**b**, **c**) plane of these pentagonal cross sections is shown in Fig. 2. A cage is built up of eight WO_6 octahedra and four PO_4 tetrahedra and is surrounded by 18 O atoms. The O atoms form eight windows between two adjacent WO_3-type slabs; four of these windows are diamond-shaped and four pentagonally shaped (Fig. 3). Equivalent cages are connected to each other through these pentagonal windows at different levels along **a**. From the centre of an O18 cage, distances to the O atoms range from 2.34 to 3.67 Å. It may therefore be quite possible to insert small cations (*e.g.* Li^+, Na^+, K^+ *etc.*) in these cages. The syntheses of such new phases are now in progress. In the present work it has been verified that no significant electron density occurs in the O_{18} cages.

3.2. *Electron microscopy study*

Preliminary studies of several crystals by electron microscopy confirmed how difficult it is to stabilize

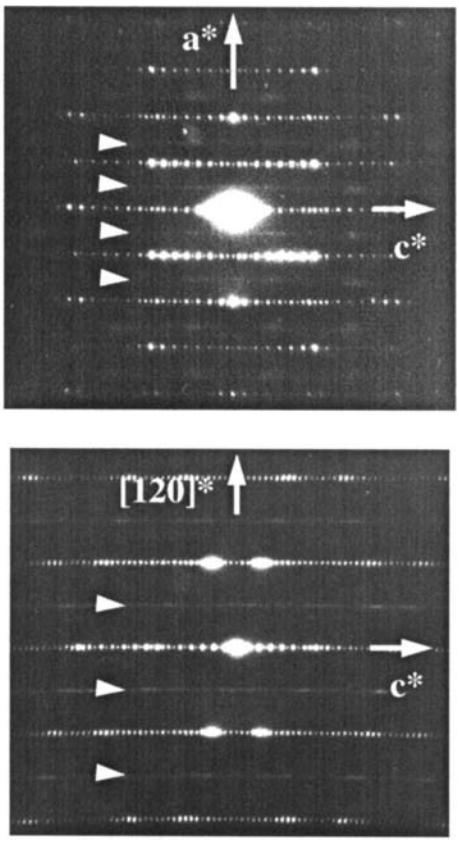

Fig. 5. ED patterns showing diffuse satellites which involve a doubling of the **a** parameter.

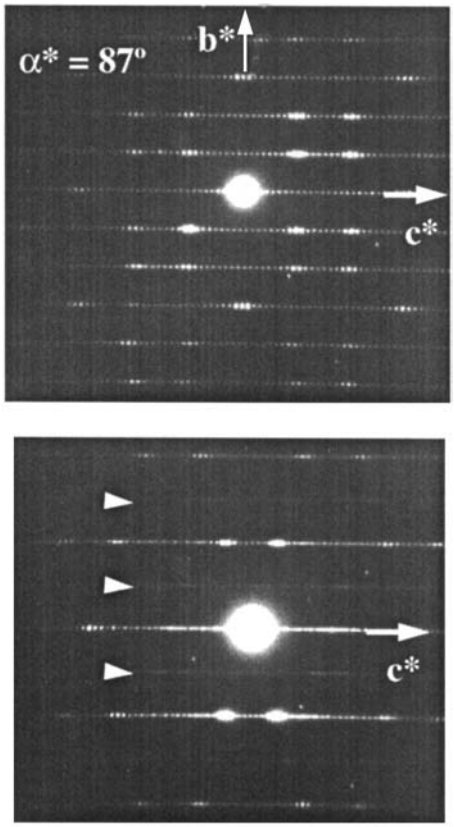

Fig. 6. [100] ED patterns of a crystal showing monoclinic symmetry: $\alpha = 93°$. The *h*2*hl* ED pattern also shows diffuse satellite involving a doubling of the **a** parameter.

almost perfect crystals of high members of the $MPTB_p$ family. Many fragments were identified as undesired high-m members (m = 10 or 11) or as an irregular intergrowth of high members, as indicated by the formation of diffuse streaks parallel to the **c*** axis. Some well crystallized m = 12 fragments were also characterized.

Electron diffraction results on the first single crystal were in agreement with those of the X-ray investigation. Again, no satellite reflections were observed, as can be seen in the ED patterns in Fig. 4. In order to carry out a complete characterization by electron diffraction, either reconstruction of the reciprocal space was performed or several crystallographic planes were directly observed for each fragment. It was observed that satellite reflections could be seen in different crystal fragments, the intensities of which varied from almost invisible to rather bright; these satellite reflections were always accompanied with diffusion phenomena (Fig. 5). If obviously these satellites result from a doubling of the **a** parameter, it is impossible to characterize the modulation vector along the **c** axis as a consequence of this diffusion. The modulation vector is expected to be half the length of the reciprocal parameter, as previously shown from diffuse X-ray scattering measurements (Ottolenghi & Pouget, 1996). Similar results have been reported elsewhere (Yan *et al.*, 1995) for a modulated m = 12 sample doped with Ge. In this case the presence of discommensurations (DC) observed directly by dark-field TEM (transmission electron microscopy) suggests that the components of the modulation wavevector are not exactly $(\frac{1}{2}, 0, 0)$, but $(\frac{1}{2} + \varepsilon, 0, 0)$, with $0 < \varepsilon \leq 0.02$. Another interesting result was deduced from electron diffraction observations of a crystal which showed satellites. This had monoclinic symmetry (Fig. 6), but with parameters close to those of the m = 12 structure. The monoclinic distortion is observed between the **b** and **c** parameters, with an α angle close to 93° (Fig. 6). This could be interpreted as a monoclinic m = 12 term, *i.e.* the regular intergrowth of m = 11 and m = 13 terms, in a

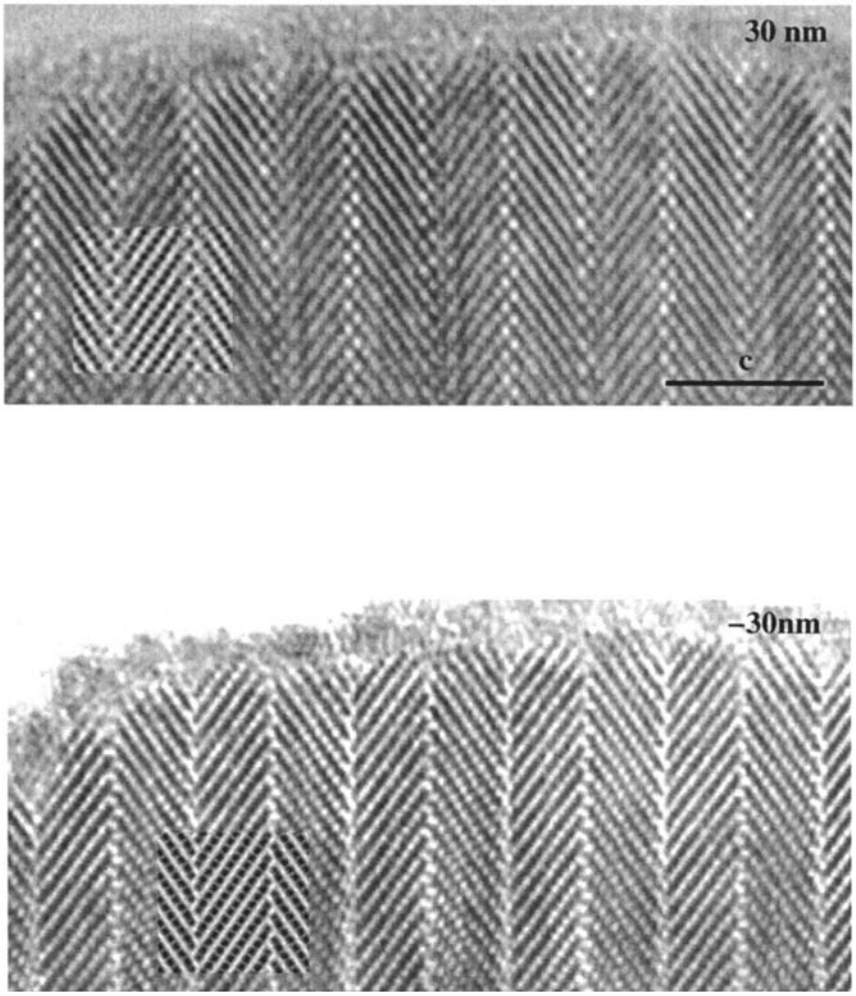

Fig. 7. [100] HREM images taken for two typical focus values. On the lower left part are inset calculated images with the following parameters: high-voltage V = 200 kV, spherical aberration constant Cs = 0.4 mm, divergence half-angle α = 0.85 mrad, spread of focus 10 nm, crystal thickness T = 3.2 nm.

similar way to the fifth member of the family, which also has monoclinic symmetry and forms by the regular intergrowth of $m = 4$ and $m = 6$ members (Benmoussa *et al.*, 1982). In fact, this latter intergrowth is quite irregular and weak diffuse streaks can also be observed parallel to the **c*** axis. Unfortunately, such crystals could not be characterized by high-resolution electron microscopy, but geometric considerations allow us to calculate the theoretical parameters of such a regular intergrowth: when two slabs with a different width (m and m') are intergrown in a regular manner, described by the following formulation, $(PO_2)(WO_3)_m(PO_2)$–$(PO_2)(WO_3)_{m'}(PO_2)$, the new periodicity (d_{001}) corresponds to the width of both slabs measured perpendicularly to the (**a**, **b**) plane

$$d_{001} = c_m/2 + c'_m/2 = [(m/2)a_p \cos 35.3 + K][(m/2)a_p \cos 35.3 + K],$$

where $a_p = 3.8$ Å, $K = 2.45$ Å ('PO_4' width) and 35.3° corresponds to the inclination of the 'WO_3' links from the ideal perovskite.

Since m and m' are different, the resulting cell will show monoclinic symmetry whose parameters can be approximated by

$$\tan \alpha_{th} \simeq \{[(m + m')/2]a_p \cos 35.3 + 2K\}/\{[(m' - m)/p]a_p \cos 35.3\}$$
$$c_{th} \simeq \{[(m + m')/2]a_p \cos 35.3 + 2K\}/\sin \alpha_{th}$$
$$a_{th} \simeq a_p(2)^{1/2}$$
$$b_{th} \simeq a_p(3)^{1/2}.$$

In our case we obtain approximate parameters $a \simeq 5.4$, $b \simeq 6.6$, $c \simeq 42.2$ Å and $\alpha \simeq 93°$; these agree closely with our observations. It would thus appear that a regular $m = 11 - m = 13$ intergrowth can be stabilized.

High-resolution images usually show a regular contrast in the $m = 12$ orthorhombic structure. Fig. 7 shows two [100] images with a typical focus value. On the 30 nm focus micrograph, high electron density zones are highlighted such that bright ribbons are related to W and O atoms in the equatorial plane of the WO_6 octahedra and the big bright dots in zigzag formation parallel to the **b** direction correspond to the PO_4 tetrahedra. The large dark dots in a zigzag arrangement parallel to **b** are related to the pentagonal tunnels and the ribbon of dark dots corresponds to the oxygen apices of the WO_6 octahedra. In the −30 nm focus micrograph low electron density zones are highlighted: the bright ribbons correspond to the perovskite-type tunnels and the oxygen apices of the WO_6 octahedra, and the large dark dots which adopt a zigzag arrangement are the W atoms. On slightly thicker areas, bright dots are resolved better and relate only to the oxygen apices of the WO_6 octahedra which lie between two rows of bright zigzags corresponding to the O atoms of the phosphate groups.

A rather new feature seen here is the frequent occurrence of intergrowth defects with another member of the $MPTB_h$ family (Fig. 8). On some areas of the crystal, and near its edge, modulations in the contrast are observed in the middle of the perovskite slabs. Compared with previous observations in the $MPTB_h$ series, it is most probable that the bright contrast can be related to an extra monophosphate plane forming hexagonal tunnels. This extra plane does not induce a

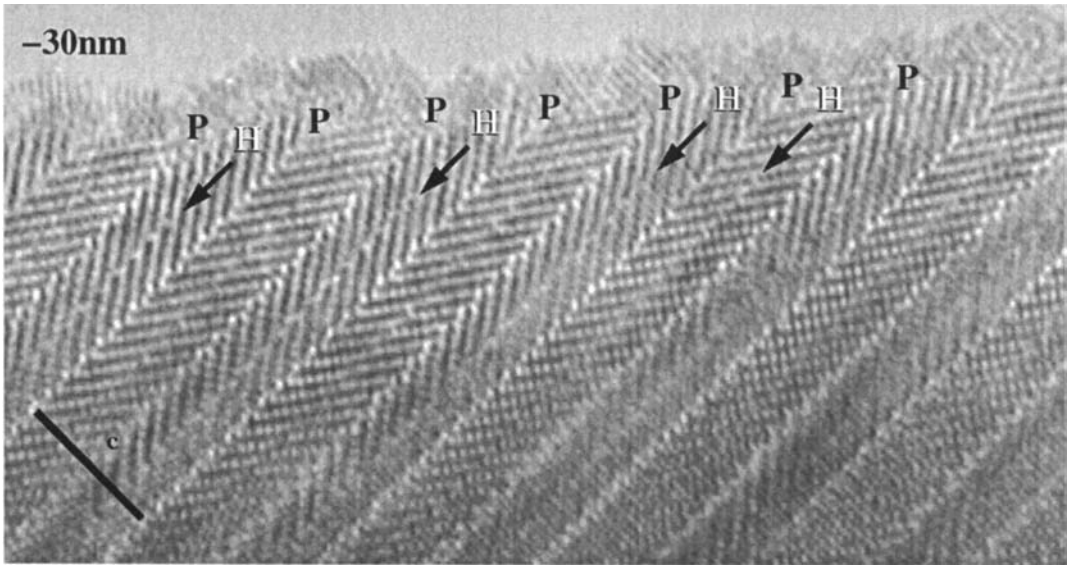

Fig. 8. [100] HREM image of another region of the previous crystal showing modulation of the contrast inside the perovskite slab (arrowed). **P** and **H**, respectively, indicate pentagonal- and hexagonal-type tunnels.

change in the direction of the octahedron ribbon. However, this feature is not widespread and it is probable that the extra monophosphate planes do not run along the entire thickness of the slab. Indeed, it has been shown in previous studies of the $MPTB_p$ series that rows of monophosphate planes forming hexagonal tunnels can easily stop inside a perovskite slab along both **a** and **b** directions (Domengès *et al.*, 1984). This phenomenon should not greatly affect the physical macroscopic properties of the compound.

3.3. *W and P atoms*

Inside each of the six WO_6 octahedra of a chain in a slab, the W atom is displaced from the centre of its octahedron. Moving along a chain, the W atom is displaced from one edge of a chain to the other, towards the middle part of the slab; this displacement is greater for W(1) and W(6) ($\delta \simeq 0.25$ Å) near the PO_4 tetrahedra than for W(4) ($\delta \simeq 0.05$ Å) in the middle of a slab. Short and long bonds alternate along the length of a chain, and are ~1.75–1.85 Å for the shortest distances and 2.00–2.10 Å for the longest. In a perpendicular plane (Fig. 9) various interatomic O—W—O chains can be seen; these are either linear or in a zigzag formation, but in both cases the chains are composed of alternate short and long W—O bonds. The dispersion of the six W—O distances in each octahedron (Fig. 10 and Table 3) is also exhibited by the m = 6, 7 and 8 members of the series (Roussel *et al.*, 1996) with a mean value of 1.92 Å. In the centre of the slabs the six W(4)—O distances are close to the mean distance. On the edges of the slabs, however, the large variation of the W(1)—O and W(6)—O distances involves a 3 + 3 split of the W environment into short and long bonds. This distortion becomes progressively greater on moving from the central octahedra to the edges. The atomic position of O(4) has been verified. However, it is notable that the W(1)—O(4) distance is slightly short (1.73 Å) and the W(6)—O(4) slightly long, albeit with a greater value of standard uncertainty (0.03 Å). These values do not permit a meaningful calculation of the oxidation state of the six independent W atoms. For the W atoms on the edges of the WO_3 slabs which show a pronounced dispersion of W—O distances, we can verify that the mean oxidation state is near 6. In contrast, in the middle part of the slab, where the six W—O distances are all close to the mean value (1.92 Å), it is probable that the bonds have a more covalent character resulting from orbital overlaps, and thus electronic delocalization will be more prominent. Note that, although the central octahedra appear almost regular, they are, in fact, slightly distorted. This can be seen more clearly in Fig. 11 where the O—O distances are distributed about their mean value 2.7 Å.

The displacement of the W atoms does not seem to influence their thermal motion, as shown from the tensor components of their thermal vibration para-

Table 3. *Main interatomic distances (Å)*

W(1)—O(1)	1.98 (2)	W(4)—O(14)	1.92 (3)
W(1)—O(2)	2.08 (3)	W(4)—O(15)	1.91 (2)
W(1)—O(3)	2.02 (3)	W(4)—O(16)	1.92 (2)
W(1)—O(4)	1.73 (3)	W(4)—O(17)	1.86 (2)
W(1)—O(5)	1.84 (3)	W(4)—O(17)	1.91 (2)
W(1)—O(6)	1.81 (2)	W(4)—O(18)	1.94 (2)
W(2)—O(6)	1.97 (2)	W(5)—O(9)	2.02 (3)
W(2)—O(7)	2.03 (3)	W(5)—O(10)	1.98 (2)
W(2)—O(8)	1.98 (3)	W(5)—O(12)	1.85 (3)
W(2)—O(9)	1.79 (3)	W(5)—O(13)	1.84 (3)
W(2)—O(10)	1.83 (2)	W(5)—O(18)	1.83 (2)
W(2)—O(11)	1.78 (2)	W(5)—O(19)	1.99 (2)
W(3)—O(11)	2.00 (2)	W(6)—O(4)	2.09 (3)
W(3)—O(12)	1.98 (3)	W(6)—O(5)	2.03 (3)
W(3)—O(13)	1.91 (3)	W(6)—O(7)	1.78 (3)
W(3)—O(14)	1.88 (3)	W(6)—O(8)	1.81 (3)
W(3)—O(15)	1.86 (3)	W(6)—O(19)	1.84 (2)
W(3)—O(16)	1.84 (2)	W(6)—O(20)	2.01 (2)
P—O(1)	1.52 (2)	P—O(3)	1.55 (3)
P—O(2)	1.53 (3)	P—O(20)	1.57 (2)

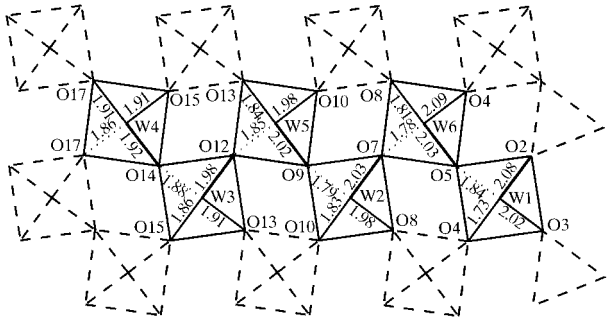

Fig. 9. O—W—O chains showing alternative long and short interatomic distances (Å).

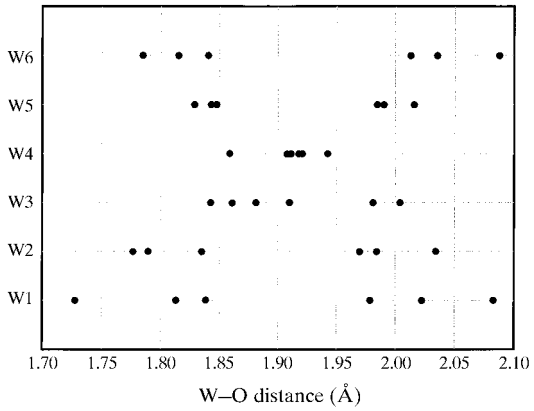

Fig. 10. Dispersion of the W—O distances observed for $P_4W_{24}O_{80}$ in a chain of six WO_6 octahedra. W(4)O_6 is just in the middle of a slab, W(6)O_6 is bound to one PO_4 tetrahedron, whereas W(1)O_6 is connected to three PO_4 tetrahedra.

Table 4. *W thermal motion analysis*

U^1, U^2 and U^3 are the mean squared displacement along the three axes of the ellipsoid. φ_x, φ_y and φ_z are the angles of the long axis with respect to **a**, **b** and **c**.

	U^{11}	U^{22}	U^{33}	U^{12}	U^{13}	U^{23}
W(1)	0.0084 (4)	0.0081 (2)	0.005773 (5)	0.0055 (8)	−0.0043 (1)	−0.00256 (3)
	U^1 = 0.016 Å^2	U^2 = 0.002 Å^2	U^3 = 0.004 Å^2	φ_x = 50°	φ_y = 50°	φ_z = 120°
W(2)	0.0092 (5)	0.0075 (2)	0.007036 (5)	0.0045 (9)	−0.0056 (1)	−0.00156 (3)
	U^1 = 0.016 Å^2	U^2 = 0.002 Å^2	U^3 = 0.006 Å^2	φ_x = 40°	φ_y = 60°	φ_z = 120°
W(3)	0.0110 (5)	0.0099 (2)	0.008389 (5)	−0.002 (1)	0.0042 (2)	−0.00233 (2)
	U^1 = 0.016 Å^2	U^2 = 0.005 Å^2	U^3 = 0.009 Å^2	φ_x = 50°	φ_y = 120°	φ_z = 60°
W(4)	0.0051 (5)	0.0115 (2)	0.008840 (5)	0.0011 (6)	−0.00503 (9)	−0.00196 (3)
	U^1 = 0.014 Å^2	U^2 = 0.002 Å^2	U^3 = 0.01 Å^2	φ_x = 60°	φ_y = 50°	φ_z = 130°
W(5)	0.0099 (7)	0.0088 (2)	0.007397 (6)	−0.0026 (6)	0.00597 (9)	−0.00101 (3)
	U^1 = 0.016 Å^2	U^2 = 0.002 Å^2	U^3 = 0.008 Å^2	φ_x = 40°	φ_y = 70°	φ_z = 120°
W(6)	0.0093 (6)	0.0066 (2)	0.006494 (5)	−0.0027 (7)	0.0019 (1)	−0.00130 (3)
	U^1 = 0.012 Å^2	U^2 = 0.005 Å^2	U^3 = 0.005 Å^2	φ_x = 40°	φ_y = 60°	φ_z = 110°

meters (Table 4). All the thermal ellipsoids of W are well defined and almost identical, with a long axis located in a plane perpendicular to the main direction of a chain of six WO_6 octahedra. For most of the octahedra, the long axis occurs between two O atoms along a diagonal of the octahedron, the short axis is in the same plane along the other diagonal and the other axis is oriented along the length of the chain. As an example, W(1) is linked to both a PO_4 tetrahedron and a W(2)O_6 octahedron *via* O(1) and O(6), respectively; its thermal ellipsoid has long and short axes, which are approximately directed along O(3)—O(5) and O(2)—O(4). W(3) is unique in that its ellipsoid has its long axis parallel to the short axis of all the other W atoms in the same octahedral chain. Although this may not be clear from Fig. 10, we note that the W(3) environment is split 4 + 2, which suggests that displacement towards an edge of its octahedron occurs; this displacement is towards a face for all the other octahedra. It can also be noted that the orientations of the long axes of the W ellipsoids in a given chain are approximately perpendicular to the long axes in an adjacent chain.

Structural refinements of different members of the $(PO_2)_4(WO_3)_{2m}$ series show that, in general, the isotropic thermal parameters, B(P), of the P atoms are low, 0.21 (4) Å^2 for m = 6 or 0.18 (5) Å^2 for m = 7 with rather high standard uncertainties, 0.21 (10) Å^2 for m = 4 or 0.46 (11) and 0.34 (9) Å^2 for m = 5. In the title compound a refinement performed with all the variables results in a B(P) of 0.01 (7) Å^2. We have verified that if B has a value such as 0.3 Å^2, the reliability factor is unchanged and the maximum change in the calculated structure factors is only 4.3%. Moreover, the existence of local intergrowth phenomena between m = 11 and m = 13 WO_3-type slabs, as observed from the electron microscopy study, may not alter the diffraction much from that in which only m = 12 WO_3-type stacking occurs.

In this case the P site refined in the calculation should be replaced occasionally in the actual structure by a W atom. Thus, the thermal factor of P tends to decrease to take this partial electronic density increase into account.

3.4. *Absolute structural configuration*

Since the space group of $P_4W_{24}O_{80}$, $P2_12_12_1$, is enantiomorphous, two non-superimposable structural models are valid; one has coordinates x, y and z and the other coordinates $-x$, $-y$ and $-z$. These two atomic arrangements are related by an inversion centre (it is easier, in this instance, to imagine that they are an object and its image in a mirror). Let us consider a WO_3-type slab as it appears in Fig. 2. Such a slab is built up of parallel chains of six WO_6 octahedra with PO_4 tetrahedra on each side which share three of their apices with three different octahedra of the slab. The remaining apex of the PO_4 tetrahedra connects two adjacent slabs. The polyhedra within a slab are somewhat rigid, but there is some flexibility between adjacent slabs. Two successive slabs are related by 2_1 screw axes running

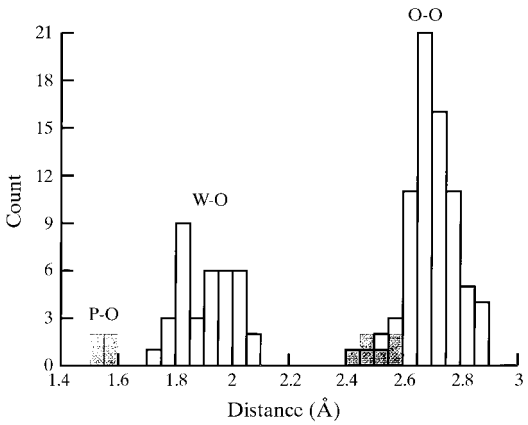

Fig. 11. Histogram of the interatomic distances. Shaded areas are related to PO_4 tetrahedra.

parallel to either **b** or **c**, producing the model depicted in Fig. 2. In this model a tilting of all the polyhedra is brought about by the non-centrosymmetric character of the crystal. The enantiomorphic twin of this model can be visualized by considering that the polyhedra tilt in the opposite direction, leading to a model which is the mirror image of the original. Note that the two models can be related through the PO_4 tetrahedra, as happens both for $P_4W_4O_{20}$ (m = 2) and for $P_4W_{14}O_{50}$ (m = 7), whose space groups both contain an n-glide.

Calculations have been carried out to check the validity of both enantiomorphs using anomalous scattering to determine the correct model. Simply changing x, y, z to $-x, -y, -z$ for all coordinates induces relatively large increases (up to 16%) in the calculated structure factors (F_c), thus illustrating the influence of the dispersion terms on the F_c values. It was found that 34 reflections have a relative variation $\Delta F_c/F_{c,\mathrm{av}}$ greater than 0.05 and for 8 reflections this variation is greater than 0.10. However, in these cases only reflections of weak intensity are involved. Refinement of the $-x, -y, -z$ coordinates results in R factors (R = 0.0291, wR = 0.0275) which are only slightly greater than those obtained with refinement using x, y, z. The largest values of the relative difference between the calculated structure factor $|F_{c1} - F_{c2}|/F_{c,\mathrm{av}}$ for the same (hkl) are listed in Table 5. As the corresponding observed structure factor F_o is highly significant for these reflections, the comparison is instructive. Most of the values are better when x, y, z is refined, indicating that the model with the direction of tilting which we originally proposed, rather than its enantiomorphic twin, corresponds to the absolute configuration of the structure of $P_4W_{24}O_{80}$. It should be noted, however, that the existence of a small proportion of the enantiomorphic configuration in the crystal cannot be completely ruled out.

Table 5. *Calculated structure factors for the two enantiomorphous models: xyz (F_{c1}), $-x - y - z$ (F_{c2})*

hkl	F_o	F_{c1}	F_{c2}	$\sigma(F_o)$	$\Delta F/F_c$
$65\bar{5}$	32	32	23	5	0.33
$51,\overline{27}$	42	40	35	5	0.13
$13\bar{1}$	53	53	47	1	0.12
$19\bar{1}$	46	41	37	4	0.10
$15\bar{9}$	34	31	28	3	0.10
$41\bar{6}$	68	72	65	2	0.10
$14\bar{9}$	31	28	31	3	0.10

The greatest values of $\Delta F/F_c = (|F_{c1} - F_{c2}|)/\overline{F}_c$ are listed according to descending order. For the first five lines, F_{c1} compared with F_c is more probable than F_{c2}.

4. Conclusions

Although the m = 12 member of the series $(PO_2)_4(WO_3)_{2m}$ is expected to exhibit a commensurate (0.5, 0, 0.5) modulation below 500 K, the present X-ray structural investigation and electron microscopy study lead us to conclude that crystals with or without charge-density wave (CDW) satellite reflections can be isolated at 300 K. Furthermore, it is shown that in the CDW state, the intensities of the satellite spots can vary from one crystal to another. Regions of a regular intergrowth of m = 11–13 were identified by electron microscopy.

The detailed structure of the regular form of m = 12 has been established and compared with that of other low-m members of the series (m = 4, 6, 8). One of the main differences with respect to the other members is the fact that the W atoms located at the border of the WO_3-type slabs are more displaced from the centre of their octahedra in m = 12. These displacements are at a similar distance to those found in the three polymorphs of tungsten trioxide (WO_3), which in the latter induce well known antiferroelectric (AFE) behaviour. According to Ottolenghi & Pouget (1996), the occurrence of such a WO_3-type AFE instability interacting with a CDW instability in the high-m members ($8 < m \leq 13$) could be at the origin of a strengthening of electron localization effects and could thus explain the increase of the Peierls transition temperatures with increasing m. However, structure refinements of other high-m members of the $(PO_2)_4(WO_3)_{2m}$ series and, more particularly, of the modulated m = 12 single phase are needed to verify this hypothesis.

This work was partly supported by the Human Capital and Mobility Program of the European Union under contract ERBCHRXCT940616.

References

Altomare, A., Cascarano, G., Giacovazzo, C., Guagliardi, A., Burla, M. C., Polidori, G. & Camalli, M. (1994). *J. Appl. Cryst.* **27**, 435–436.

Becker, P. J. & Coppens, P. (1974). *Acta Cryst.* A**30**, 148–153.

Benmoussa, A., Labbé, Ph., Groult, D. & Raveau, B. (1982). *J. Solid State Chem.* **44**, 318–325.

Canadell, E. & Whangbo, M. H. (1991). *Phys. Rev. B*, **43**, 1894–1902.

Creagh, D. C. & McAuley, W. J. (1992). *International Tables for Crystallography*, Vol. C, pp. 206–222. Dordrecht: Kluwer Academic Publishers.

Domengès, B., Hervieu, M., Raveau, B. & Tilley, R. J. D. (1984). *J. Solid State Chem.* **54**, 10–28.

Foury, P. & Pouget, J. P. (1993). *Int. J. Mod. Phys. B*, **7**, 3973–4003.

Giroult, J. P., Goreaud, M., Labbé, Ph. & Raveau, B. (1981). *Acta Cryst.* B**37**, 2139–2142.

Hess, C. (1997). Ph.D. thesis. Grenoble University, France.

Hess, C., Schlenker, C., Dumas, J., Greenblatt, M. & Teweldemedhin, Z. S. (1996). *Phys. Rev. B*, **54**, 4581–4588.

Labbé, Ph., Goreaud, M. & Raveau, B. (1986). *J. Solid State Chem.* **61**, 324–331.

Le Touze, C., Bonfait, G., Schlenker, C., Dumas, J., Almeida, M., Greenblatt, M. & Teweldemedhin, Z. S. (1995). *J. Phys. I Fr.* **5**, 437–442.

Maslen, E. N., Fox, A. G. & O'Keefe, M. A. (1992). *International Tables for Crystallography*, Vol. C, pp. 476–511. Dordrecht: Kluwer Academic Publishers.

Ottolenghi, A. & Pouget, J. P. (1996). *J. Phys. I Fr.* Schegolev Memorial Vol. **6**, 1059–1083.

Petricek, V. & Dusek, M. (1997). *JANA*96. Institute of Physics, Praha, Czech Republic.

Roussel, P., Labbé, Ph., Groult, D., Domengès, B., Leligny, H. & Grebille, D. (1996). *J. Solid State Chem.* **122**, 281–290.

Schlenker, C., Dumas, J., Greenblatt, M. & van Smaalen, S. (1996). *Physics and Chemistry of Low Dimensional Inorganic Conductors.* NATO ASI Series. New York: Plenum Press.

Wang, S. L., Wang, C. C. & Lii, K. H. (1989). *J. Solid State Chem.* **82**, 298–302.

Yan, Y., Kleman, M., Le Touze, C., Marcus, J., Schlenker, C. & Buffat, A. (1995). *Europhys. Lett.* **30**, 49–54.